NIH Public Access
Author Manuscript
IEEE Trans Neural Syst Rehabil Eng. Author manuscript; available in PMC 2012 July 16.

Published in final edited form as:
IEEE Trans Neural Syst Rehabil Eng. 2012 March ; 20(2): 184–197. doi:10.1109/TNSRE.2012.2189163.

A Nonlinear Model for Hippocampal Cognitive Prosthesis: Memory Facilitation by Hippocampal Ensemble Stimulation

Robert E. Hampson, IEEE [Member],
Department of Physiology, Wake Forest School of Medicine, Winston-Salem, NC 27157 USA

Dong Song, IEEE [Member],
Department of Biomedical Engineering, Viterbi School of Engineering, and the Biomedical Simulations Resource, University of Southern California, Los Angeles, CA 90089 USA

Rosa H.M. Chan, IEEE [Student Member],
Department of Biomedical Engineering, Viterbi School of Engineering, and the Biomedical Simulations Resource, University of Southern California, Los Angeles, CA 90089 USA

Andrew J. Sweatt,
Department of Physiology, Wake Forest School of Medicine, Winston-Salem, NC 27157 USA

Mitchell R. Riley,
Department of Physiology, Wake Forest School of Medicine, Winston-Salem, NC 27157 USA

Gregory A. Gerhardt,
Center for Microelectrode Technology, University of Kentucky, Lexington, KY 40506 USA

Dae C. Shin, IEEE [Member],
Department of Biomedical Engineering, Viterbi School of Engineering, and the Biomedical Simulations Resource, University of Southern California, Los Angeles, CA 90089 USA

Vasilis Z. Marmarelis, IEEE [Fellow],
Department of Biomedical Engineering, Viterbi School of Engineering, and the Biomedical Simulations Resource, University of Southern California, Los Angeles, CA 90089 USA

Theodore W. Berger, IEEE [Fellow], and
Department of Biomedical Engineering, Viterbi School of Engineering, and the Biomedical Simulations Resource, University of Southern California, Los Angeles, CA 90089 USA

Samuel A. Deadwyler, IEEE [Member]
Department of Physiology, Wake Forest School of Medicine, Winston-Salem, NC 27157 USA

Gregory A. Gerhardt: gregg@uky.edu; Theodore W. Berger: berger@bmsrs.usc.edu; Samuel A. Deadwyler: sdeadwyl@wakehealth.edu

Abstract

Collaborative investigations have characterized how multineuron hippocampal ensembles encode memory necessary for subsequent successful performance by rodents in a delayed nonmatch to sample (DNMS) task and utilized that information to provide the basis for a memory prosthesis to enhance performance. By employing a unique nonlinear dynamic multi-input/multi-output (MIMO) model, developed and adapted to hippocampal neural ensemble firing patterns derived from simultaneous recorded CA1 and CA3 activity, it was possible to extract information encoded in the sample phase necessary for successful performance in the nonmatch phase of the task. The extension of this MIMO model to online delivery of electrical stimulation delivered to the same recording loci that mimicked successful CA1 firing patterns, provided the means to increase levels of performance on a trial-by-trial basis. Inclusion of several control procedures provides evidence for the specificity of effective MIMO model generated patterns of electrical stimulation. Increased utility of the MIMO model as a prosthesis device was exhibited by the demonstration of

NIH-PA Author Manuscript
NIH-PA Author Manuscript
NIH-PA Author Manuscript

NIH-PA Author Manuscript

NIH-PA Author Manuscript

NIH-PA Author Manuscript

cumulative increases in DNMS task performance with repeated MIMO stimulation over many sessions on both stimulation and nonstimulation trials, suggesting overall system modification with continued exposure. Results reported here are compatible with and extend prior demonstrations and further support the candidacy of the MIMO model as an effective cortical prosthesis.

Keywords

Closed-loop feedback; cortical neural prosthesis; delayed memory task; hippocampal ensemble activity; neural stimulation; nonlinear mathematical model; performance enhancement

I. Introduction

The encoding of memory by brain systems has long been one of the major interests of neuroscience research since this process allows temporal bridging between events that occur at different times, as well as expectation of future circumstances based on accurate recall of prior experiences [1]. Effective memory requires recognition, categorization and detection in order to allow adequate performance in a number of conditions [2] as indicated most dramatically by circumstances such as Alzheimer's disease in which total memory loss leads to incapacitation and helplessness [3]. The brain structure most intricately involved in this process is the hippocampus, existent in all mammalian species and capable of long-term retention of goal-directed objectives [4]–[7]. Development of new technologies and brain-behavior assessments have allowed progressive insight into the process of memory formation and retrieval in this structure [8]–[13] to the extent of making it possible to formulate and test a "device" that can substitute for these functions when they are compromised by damage or disuse [17] in the same manner as other neural prostheses [14]–[16].

In order to understand the neural basis of memory in hippocampus several features of both the context in which encoding occurs as well as the functional aspects of simultaneous multineuron firing patterns must be identified, interpreted and manipulated which has been an important objective of the research described here. This entailed integrating 1) an effective operational mathematical model for online prediction of CA1 cell discharges from simultaneously recorded firing patterns of presynaptic CA3 neurons [14], [17]–[19], together with, 2) systematic recordings of hippocampal ensemble activity in a behavioral task in which trial-to-trial short-term encoding of task features was required for successful performance [20], [21]. The combining of these two approaches involved the analysis and characterization of neuronal firing patterns in CA3/CA1 hippocampal subfields that have been repeatedly subjected to mathematical nonlinear input/output analysis [22]–[25]. The culmination of these investigations [26] demonstrated that the "codes" extracted online by the multi-input/multi-output (MIMO) nonlinear model could 1) enhance performance by changing the memory requirements of the task to fit the strength of encoding and 2) replace the pharmacological induced compromised operation of hippocampus by inserting electrical stimulation patterns that mimicked natural strong codes in animals performing the same task.

In the studies reported here four additional features of MIMO model extracted firing patterns of hippocampal ensembles are demonstrated that provide further support for its application as memory prosthesis. First, the actual basis of the utility of ensemble firing patterns detected by the MIMO model is revealed in terms of how encoding of specific task events reflects likelihood of performance on a given trial. Second, it is shown that if given repeatedly on specified trials within the testing session, such facilitatory MIMO model

NIH-PA Author Manuscript

NIH-PA Author Manuscript

NIH-PA Author Manuscript

stimulation patterns can enhance performance on trials without stimulation in the same sessions and that such enhancement persists even after stimulation trials are terminated. Third, we report that similar patterns exist across animals similarly prepared and trained and can be generalized and used to improve performance via standardized stimulation patterns even if not previously recorded from the same animals. Finally, it is revealed that hippocampal firing patterns extracted online by the MIMO model and used to control and predict behavioral performance conform to the synchronized firing of cells in the ensemble that naturally successfully encode task features [27]. Collectively these findings support the feasibility of applying the current prosthetic device [26] to 1) facilitate the repair of damaged or disrupted brain-memory processes, and/or 2) enhance memory functions in circumstances where retention is weak or ineffective [14], [28]–[30].

II. Methods

1) Animals

Forty five male, Long-Evans rats (Harlan) aged 4–6 months were used as subjects. They were individually housed, allowed free access to food and water-restricted to maintain 85% of *ad libitum* body weight during testing. All animal protocols were approved by the Wake Forest School of Medicine Institutional Animal Care and Use Committee (IACUC), Association for Assessment and Accreditation of Laboratory Animal Care (AAALAC), and the National Institute of Health (NIH) Guide for the Care and Use of Laboratory Animals.

2) Apparatus

The behavioral testing apparatus for the delayed nonmatch to sample (DNMS) task is the same as reported in other studies from this laboratory [21], [22], [26], [31]–[33] and consisted of a 43 × 43 × 50 cm Plexiglas chamber with two retractable levers (left and right) positioned on either side of a water trough on the front panel [Fig. 1(a)]. A nose-poke device (photocell) was mounted in the center of the opposite back panel with a cue light positioned immediately above the nose-poke device. A video camera was mounted on the ceiling and the entire chamber was housed inside a commercially built sound-attenuated cubicle.

3) Behavioral Training Procedure

The DNMS task consisted of three main phases: Sample, Delay, and Nonmatch [Fig. 1(a)]. At the initiation of a trial, either the left or right lever was randomly (50% probability) selected and extended and the animal required to press the lever as the Sample Response (SR), which retracted the SR lever and initiated the Delay phase, signaled by the illumination of a cue light over the nosepoke photocell device on the rear panel (Fig. 1(a), Delay). At least one nosepoke was required during the delay interval which varied randomly in duration between 1–30 s on each trial during the session. After the delay timed out the cue light turned off and both levers on the front panel were extended, signaling the onset of the Nonmatch phase. A correct response in the Nonmatch phase consisted of a response on the opposite lever, a Nonmatch Response (NR) with respect to the SR, and produced a drop of water (0.4 ml) reward in the trough between the two levers. After the NR the levers were retracted for a 10.0-s intertrial interval (ITI) before a Sample lever was presented to begin the next trial. A response on the same lever as the SR (Match Response) constituted an “error” with no water delivery and the chamber house lights dimmed for 5.0 s with the next trial presented 5.0 s later. Individual performance was assessed as % correct NRs with respect to the total number of trials (100–150 per 1–2 h daily session) as well as the % correct trials as a function of delay [Fig. 1(b)].

NIH-PA Author Manuscript

NIH-PA Author Manuscript

NIH-PA Author Manuscript

4) Hippocampal Electrode Arrays

All surgical procedures conformed to NIH and AAALAC guidelines, and were performed in a rodent surgical facility approved by the Wake Forest School of Medicine IACUC. Following training to criterion performance levels in the DNMS task animals were anesthetized with ketamine (100 mg/kg) and xylazine (10 mg/kg) and placed in a stereotaxic frame. Craniotomies (25 mm diameter) were performed bilaterally over the dorsal hippocampus to provide for implantation of two identical array electrodes (Neurolinc, New York), each consisting of two rows of eight stainless steel microwires (diameter: 20 μm) positioned such that the geometric center of each electrode array was at co-ordinates 3.4 mm posterior to Bregma and 3.0 mm lateral (right or left) to midline [34]. The array was designed such that the distance between two adjacent electrodes within a row was 200 μm and between rows was 400 μm to conform to the locations of the respective CA3 and CA1 cell layers [21]. The longitudinal axis of the array of electrodes was angled 30° to the midline during implantation to conform to the orientation of the longitudinal axis of the hippocampus, with posterior electrode sites more lateral than anterior sites [Fig. 1(c)]. The electrode array was lowered in 25–100 μm steps to a depth of 3.0–4.0 mm from the cortical surface for the longer electrodes positioned in the CA3 cell layer, leaving the shorter CA1 electrodes 1.2 mm higher with tips in the CA1 layer. Extracellular neuronal spike activity was monitored from all electrodes during surgery to maximize placement in the appropriate hippocampal cell layers. After placement of the array the cranium was sealed with bone wax and dental cement and the animals treated with buprenorphine (0.01–0.05 mg/kg) for pain relief over the next 4–6 h. The scalp wound was treated periodically with Neosporin antibiotic and systemic injections of penicillin G (300 000 U, intramuscular) were given to prevent infection. Animals were allowed to recover from surgery for at least one week before continuing behavioral testing [27].

5) Electrophysiological Acquisition and Monitoring of Neural Data

Animals were connected by cable to the recording apparatus via a 32-channel headstage and harness attached to a 40-channel slip-ring commutator (Crist Instruments, Hagerstown, MD) to allow free movement in the behavioral testing chamber. Single neuron action potentials (spikes) were isolated by time-amplitude window discrimination and computer-identified individual waveform characteristics using a multi-neuron acquisition processor (MAP) (Plexon Inc., Dallas, TX). Single neuron spikes were recorded daily using waveform and firing characteristics within the task (perievent histograms) for each of the DNMP events (SR, LNP, and NR). Only isolated spike waveforms exhibiting firing rates consistent with CA1 and CA3 principal cells (i.e., 0.5–5.0 Hz baseline firing rate) and stable behavioral correlates across sessions were employed for experimental manipulations and model development [16], [20], [22], [35]–[37]. Final neuron ensembles used to analyze encoding of DNMP events consisted 15–32 single neurons, each recorded from a separate identified electrode location on the bilateral arrays [Fig. 1(c)].

6) MIMO Model

A general, nonlinear model using a Volterra kernel-based strategy for the MIMO nonlinear dynamics underlying the transformation of CA3 to CA1 spike trains was established to predict output patterns of CA1 firing pattern from input patterns of CA3 neural activity [14], [19], [38]–[40]. The spatio-temporal pattern transformations from the hippocampal CA3 region to the CA1 region are thus formulated in a manner that the MIMO system can be decomposed into a series of multiple-input, single-output (MISO) subsystems (Fig. 2) that can be expressed by the following equations

$$w=u(k,x)+a(h,y)+\varepsilon(\sigma)$$

NIH-PA Author Manuscript

NIH-PA Author Manuscript

NIH-PA Author Manuscript

$$y=\begin{cases} 0, & \text{when } w<\theta \\ 1, & \text{when } w \geq \theta \end{cases}$$

where the variables x_i and y_i represent input and output spike trains, respectively, and the hidden variable w represents the prethreshold membrane potential of the output neurons. Three physiologically plausible components are incorporated in the system: u, the synaptic potential produced by the input spike trains; a, the output spike-triggered after-potential; and ε, a Gaussian white noise term with standard deviation, σ, which accounts for both unobserved inputs and intrinsic noise of the output neuron. An output spike (y) is generated when w exceeds threshold, θ. A feedback after-potential (a) and feedback kernel (h, describing the transformation of y to a) are also triggered and then added to w. The feedforward kernel, k describes the transformation from x to u, allowing u to be expressed as a Volterra functional series of x

$$\begin{aligned} u(t)=k_0+&\sum_{n=1}^{N}\sum_{\tau=0}^{M_k}k_1^{(n)}(\tau)x_n(t \\ &-\tau)+\sum_{n=1}^{N}\sum_{\tau_1=0}^{M_k}\sum_{\tau_2=0}^{M_k}k_{2s}^{(n)}(\tau_1, \\ &\tau_2)\times x_n(t \\ &-\tau_1)x_n(t \\ &-\tau_2)+\sum_{n_1=1}^{N}\sum_{n_2=1}^{n_1-1}\sum_{\tau_1=0}^{M_k}\sum_{\tau_2=0}^{M_k}k_{2x}^{(n_1,n_2)}(\tau_1,\tau_2)\times x_{n_1}(t \\ &-\tau_1)x_{n_2}(t \\ &-\tau_2)+\sum_{n=1}^{N}\sum_{\tau_1=0}^{M_k}\sum_{\tau_2=0}^{M_k}\sum_{\tau_3=0}^{M_k}k_{3s}^{(n)}(\tau_1, \\ &\tau_2,\tau_3)\times x_n(t \\ &-\tau_1)x_n(t \\ &-\tau_2)x_n(t-\tau_3)+\cdots \end{aligned}$$

where N is the number of inputs, with M_k equal to the "memory" length (in time bins) of the feedforward process. The zero order kernel, k_0, is the "background" or baseline value of u with no input. First-, second-, and third-order self-kernels, $k1^{(n)}$, $k_2^{(n)}$, and $k_3^{(n)}$, describe the first-order linear, as well as second- and third-order nonlinear relations between the nth input x_n and u, respectively. Second-order cross-kernels, $k_2^{(n1,n2)}$, describe the nonlinear interactions between each unique pair of inputs (x_{n1} and x_{n2}) as they affect u. The output feedback variable, a, from the MISO subsystem above is expressed as

$$a(t)=\sum_{\tau=1}^{M_h}h(\tau)y(t-\tau)$$

where M_h is the memory length (in time bins) of the feedback process, and h is the linear feedback kernel.

NIH-PA Author Manuscript

NIH-PA Author Manuscript

NIH-PA Author Manuscript

The full model describes the transformation of third-order (i.e., triplets) of temporal spike train intervals for each input, and second-order (i.e., pairs) temporal intervals for any of two interacting inputs, into output spike trains, taking into account noise and output spike-triggered feedback due to circuitry and/or membrane biophysics, as well as threshold differences specific to each neuron. In order to reduce the number of open parameters to be estimated, orthonormal Laguerre basis functions [17] were used to expand the k and h terms. Given the Gaussian noise term and the threshold, this model operates as a special case of the Generalized Laguerre–Volterra Model (GLVM) employing a *probit* link function [24], [41], [42]; and uses an iterative reweighted least-squares method [18] to estimate all model parameters. Threshold, θ, and noise deviation, σ, are redundant variables indirectly obtained through variable transformation [24], [41], [42]. The stochastic nature of the system allows validation of model estimates using a Kolmogorov–Smirnov test based on time-rescaling [43]. Code Strength is computed from the ensemble firing rate multiplied by the MIMO coefficients for each single trial. The coefficients are the same for each trial; however, the firing of each neuron varies on each trial. Thus, Code Strength yields a continuous measure of variability in ensemble firing as well as correspondence between neural activity on single trials versus the mean across Correct trials for Left versus Right SR; with weak (< 1.0) scores corresponding to errors and strong (> 2.0) scores corresponding to correct DNMS performance.

7) Prediction of CA1 Firing Using MIMO Model

CA1 output predictions from the MIMO model were computed across 3–5 consecutive DNMS sessions for each animal. The MIMO model accurately predicted CA1 (output) spike trains based on CA3 (input) spike trains on *strong* and *weak* SR code trials (Fig. 2, lower right), requiring at least second-order self-kernels (k_{2S}) to sufficiently capture the CA3-CA1 nonlinear dynamics. MIMO detected single trials were identified as consistent with *strong* and *weak* SR codes based on correlation with successful DNMS performance. MIMO-derived *strong* SR code CA1 firing patterns showed common features across animals and were thus averaged to produce a "Generic" CA1 *strong* SR code pattern which was tested in the same manner as MIMO derived patterns during CA1 stimulation trials.

8) Computation of MIMO Code Strength

CA3 and CA1 neural firing patterns were defined as strong codes in terms of behavioral performance. Trials that were correct at the longest DNMS trial delays (21–30 s) were classified as Strong Codes, while trials that are errors at short delays (< 15 s) were classified as Weak Codes. Kernels of the MIMO model were computed using only Left and Right Strong Code trials, so that the model prediction of CA1 firing generated Strong Codes for Left and Right trials. Within the MIMO model, individual trial SR Codes were identified and scored by computing the Pearson product-moment cross-correlation of each MIMO Model CA1 prediction with actual CA1 firing, and normalizing the resultant scores to mean = 0 with standard deviation = ±1.0. This produced a bimodal distribution of scores with peaks at approximately −2.0 and +2.0, representing the mean scores for Left and Right trials, respectively. The absolute value of this distribution, scaled from 0 to 3.5 with a peak between 1.5 and 2.5, is reported here as "Code Strength" (Figs. 2 and 4). Strong Codes are thus trials with > scores one standard deviation above the mean (peak) of the distribution, while Weak Codes are those scores less than one standard deviation below the peak of the distribution.

9) MIMO Generated Electrical Stimulation of CA1 Neurons

A custom built 16-channel stimulator (Triangle BioSystems Inc., Durham, NC) was utilized to deliver patterns of electrical pulses to CA1 electrodes bilaterally in both hippocampal arrays. The stimulator delivered digital-to-analog (D/A) converted biphasic output pulses to

NIH-PA Author Manuscript

NIH-PA Author Manuscript

NIH-PA Author Manuscript

the eight CA1 electrodes in each single array. Each D/A output channel delivered one-half of a symmetric biphasic stimulation pulse of 1.0 ms duration to a pair of adjacent electrodes in CA1 allowing bipolar stimulation that was isolated from other electrodes on the same array. The biphasic stimulator pulses were electronically gated to produce square constant voltage outputs in the range of 0.1 to 15 V (20 – 100 μA) in 0.1 V increments with a minimum interpulse interval of 50 ms on a given channel. The range of parameters typically employed on a single MIMO output channel was: biphasic, 1.0–4.0 V p-p, 1.0 ms, ≤ 20.0 Hz. Stimulation patterns consisted of pulses delivered to eight pairs of CA1 electrodes in trains of 1.5–3.0 s duration during performance of the SR. Real-time lag between CA3 recording and MIMO calculation and stimulation was approximately 100 ms. Controls consisted of 1) delivery of trains of the same pulse intensities that were *randomized* with respect to location and timing between channels by shifting the coefficients of the MIMO model, or 2) by delivering effective SR patterns at different times periods during the trial other than coincident with the SR [26].

III. Results

Analyses of hippocampal neuronal activity in rodents performing the DNMS memory task have been conducted over a number of years and have yielded trial-specific patterns of firing by ensembles of neurons recorded in a specific spatiotemporal context [20]–[22], [31], [33], [44]–[47]. Fig. 1(a) shows the DNMS task in which the rat was required to make a “Sample” lever response (SR) at the start of the trial when either the Right or Left lever was presented, and retain the position of the lever during a subsequent delay interval that varied randomly in duration from 1–30 s on different trials, in order to make the correct “Nonmatch” response (NR) by pressing the lever in the opposite position to the SR when both levers were presented after the delay timed out. Fig. 1(b) shows that DNMS performance accuracy (% correct NRs) decreased uniformly across animals ($n = 25$) as a direct function of the duration (1–30 s) of the intervening delay interval. A correlated behavioral measure, mean latency to make the NR from the time that both levers were presented in the Nonmatch phase increased as a function of delay duration and was inversely related to performance accuracy [Fig. 1(b)]. Electrophysiological recording of hippocampal neural activity during the DNMS task employed custom designed arrays of microwire (20 μm) electrodes implanted bilaterally in the dorsal hippocampus [21], [22] to provide single neuron firing data from eight pairs of CA3-CA1 probes aligned at 200 μm intervals along the longitudinal axis of hippocampus [21], [33].

We have recently utilized the MIMO nonlinear mathematical model for analysis of CA3/CA1 ensemble firing to provide real-time assessment of ensemble “SR codes” to predict CA1 output patterns based on the CA3 neural firing inputs [Fig. 1(c)] to the model [26]. The model was used to determine the temporal firing relationships between spike occurrences recorded in CA3 (left) and CA1 [CA1 Actual, Fig. 1(c)] on correct DNMS trials irrespective of duration of delay. Color contour displays of the rate of firing of the respective CA3 and CA1 neurons recorded from the hippocampal electrode array 3.0 s prior to occurrence of the SR at each spatial position of the Sample lever, are shown in Fig. 1(c). Both the recorded (Actual) and MIMO model predicted outputs of at the same CA1 cell locations are shown for each position of the SR corresponding to different trial types. The MIMO model therefore: 1) receives presynaptic inputs from CA3 cell discharges (Fig. 1(c), *CA3 Input*) and 2) calculates outputs for postsynaptic CA1 cells based on those inputs (Fig. 1(c), *CA1 Prediction*) via putative monosynaptic, Schaffer collateral connections [48]. The recorded firing of CA1 neurons over the same trials in which CA3 activity was used to teach the model and extract MIMO coefficients, is shown for comparison in Fig. 1(c) (*CA1 Actual*) to illustrate similarity to the MIMO model output. Hence, the MIMO model extraction of nonlinear coupling between CA3 and CA1 neuronal spike events provides the basis for

NIH-PA Author Manuscript

NIH-PA Author Manuscript

NIH-PA Author Manuscript

online "prediction" of CA1 (output) neuron firing from simultaneously recorded CA3 (input) cell activity in the same hemisphere.

1) DNMS Performance Accuracy and MIMO Model-Predicted Firing Patterns

The MIMO model also provided a means of identifying "strong" versus "weak" SR encoding on individual trials [26]. Since the MIMO model was developed using the SR firing on correct Left or Right DNMS trials, its predictions represent CA1 firing patterns highly likely to be rewarded on the same trial (i.e., "strong SR codes"). The rate contour maps at the top of Fig. 2(a) compare the recorded CA1 firing (*Actual*) to MIMO-predicted CA1 firing (*Model: Strong Code*) on successfully performed Left DNMS trials and at the bottom this same comparison is made for errors on left trials (*Model: Weak Codes*). Contour maps were computed as $x \bullet w_{\text{Left}}$, where x = ensemble firing rates by neuron and time, and w_{Left} = the weighting coefficients derived from the MIMO model that generated the mean firing pattern associated with correct Left trials. The graph in the middle [Fig. 2(a)] plots behavioral performance on left trials of different delay durations as a function of differing SR "code strength." The weighted firing rate Code strengths in Fig. 2(a) were computed as the correlation between the actual firing pattern and MIMO-predicted Left Correct SR firing. These scores were normalized (mean = 0, standard deviation = 1) such that a "strong code" ($x_{\text{Left}} \bullet w_{\text{Left}} = 2.5$) yielded maximal performance. For MIMO model derived Strong SR code patterns with a "code strength" of 2.5 (Fig. 2(a), red triangles) correct performance was > 90% at nearly all delays. However if a CA1 firing pattern for a Right correct trial occurred on a Left trial (Fig. 2(a) bottom) this represented the least correlation with the Left trial Strong code and resulting in a very "weak code" ($x_{\text{Right}} \bullet w_{\text{Left}} = 0.5$) for that type of trial. Since the weakest code for a Left trial is the strong code for a Right trial this should correlate with the worst possible performance as a function of delay, which is shown at a strength 0.5 in Fig. 2(a). Fig. 2(b) shows examples of intermediate levels of code strength associated with different levels of performance in terms of codes that result from a lack of exact matches to the MIMO model prediction of CA1 derived from strong codes. This is because the firing of the CA3 input contains spikes at spatiotemporal locations that do not match the firing on correct trials to different degrees ranging from similar but not the same as strong codes to patterns that approach that appropriate for the opposite type of trial (weak codes). It is clear from Fig. 2(b) that the transformation from Strong to Weak codes involves a lack of clustering of synchronous firing which is indicated by the more or less random dispersion across the CA1 recording sites. Interestingly therefore the MIMO derived code associated with normal DNMS performance [Fig. 1(b)] is most similar to the code strength curve in Fig. 2(b) (green curve) that yields a nearly random weighted firing ($[x_{\text{Left}} : x_{\text{Right}}] \bullet w_{\text{Left}}$) as shown in Model Normal Code map indicating that normal performance of the task is associated with SR codes for the correct and incorrect lever on any given trial This mixture of cell type firing across trials during DNMS sessions has been reported before (31) and shows that the strong codes were composed of appropriate cell types for that trial and that weak codes consist of cell firing that is appropriate for the opposite trial type.

2) Enhanced DNMS Performance With CA1 Stimulation Derived From MIMO Model Patterns

To assess the ability to apply the MIMO model of hippocampal ensemble processing as a cortical prosthesis [26], these same CA1 output predictions from CA3 cell firing were transformed online into simultaneous electrical stimulation patterns (1.0 ms biphasic pulses 20–100 μA) delivered bilaterally to the same CA1 electrode locations in the hippocampal arrays during the SR [Fig. 3(a)]. The patterns of electrical stimulation were specific for *strong SR code* for each lever position (right or left), as shown in Fig. 1(c). Under normal DNMS testing conditions MIMO model stimulation facilitated performance in relation to trials in which stimulation was not delivered by the model. Fig. 3(b) shows that such stimulation produced a significant ($F_{(6,1057)} = 12.7$, $p < 0.001$) increase in performance (Fig.

NIH-PA Author Manuscript

NIH-PA Author Manuscript

NIH-PA Author Manuscript

3(b), *MIMO Stim*, $n = 9$ animals) on trials with delays > 10 s compared to similar trials in the same sessions without stimulation *(Control)*. Since the stimulation patterns were specific for the right or left lever, the effectiveness of the stimulation was not related to: 1) mere increases in neuron firing rate (Fig. 2), 2) presence or absence of stimulation as a cue and 3) differences in stimulation intensity [26]. A further demonstration of specificity was demonstrated by delivery of the Left CA1 stimulation pattern on Right lever DNMS trials (and vice-versa) which resulted in a significant ($F_{(6,1057)} = 8.3$, $p < 0.001$) *impairment* of DNMS performance relative to control levels (Fig. 3(b), *Reversed Stim*) and suggests that the animals were biased to respond on the *opposite* lever as encoded by the pattern of stimulation [Fig. 3(c)]. Finally, delivering a randomized stimulation pattern by "scrambling" the coefficients of the MIMO model did not facilitate performance ($F_{(6,1057)} = 0.7$, n.s.) in the same manner as strong code stimulation indicating that delivery of electrical current alone irrespective of pattern was not sufficient to improve performance. Also stimulation with scrambled coefficients did not impair performance below normal control levels (Fig. 3(b), *Scrambled Coeff*) which is consistent with the results shown in Fig. 2(b) in which there is a similarity with "Normal Intermediate Codes" associated with nonfacilitated performance of the task under normal conditions. The randomized (scrambled) coefficient procedure imposes a stimulation pattern which can activate both appropriate and inappropriate cell types, which is similar to the normal code intermediate firing patterns shown in Fig. 2(b). Therefore, on scrambled stimulation trials the hippocampus is activated in the same manner (Fig. 3) under normal performance conditions when neither a strong or weak code is present on the trial (Fig. 2(b), Intermediate Normal code).

3) Cumulative Effects of Repeated Strong Code CA1 Stimulation on DNMS Performance

Another feature of MIMO model stimulation patterns that could serve an extrapolated benefit as a cortical prosthesis was examined with respect to repetition of *strong SR code* stimulation procedures over several testing sessions. In this context individualized MIMO model stimulation patterns [Fig. 1(c)] as well as a Generic (mean across animals) MIMO *strong SR* code stimulation pattern (Fig. 2), were both tested (in different animals) to assess the cumulative effects of MIMO stimulation over several sessions. A unique aspect of this assessment was that the effect of stimulation delivered on selected (20%–40%) trials in the session (delays 16–30 s) was also evaluated with respect to performance on trials in the same sessions in which no stimulation occurred. As previously utilized for animals with compromised hippocampal activity [26], a "Generic" *strong* SR code stimulation pattern, derived across several individual animal strong code patterns, was delivered to CA1 at the time of the SR. Comparison of the open symbols in Fig. 4(a) shows that a marked increase in overall mean % correct performance ($n = 8$ animals) occurred rapidly on across trials and sessions for both stimulation conditions. Mean performance on nonstimulation trials increased at slower rate but was consistent over 240–400 trials in the same sessions [red and blue curves, Fig. 4(a)]. Such changes over time were markedly different from the flat cumulative performance curves for animals ($n = 10$) with no exposure to MIMO model stimulation trials during the same time period [Control, Fig. 4(a)]. Both stimulation patterns produced facilitation of performance on nonstimulated trials in the same sessions, however individualized MIMO Stim patterns produced a faster facilitation (slope = 24%/day, R = 0.79, $F_{(1,88)} = 39.10$, $p < 0.001$) than Generic Stim (slope = 1.5%/day, R = 0.74, $F_{(1,88)} = 44.9$, $p < 0.001$) as shown in Fig. 4(a). Animals that received individualized MIMO Stim patterns also showed a slower decline in performance (slope − 1.4%/day, R = 0.82, $F_{(1,88)} = 27.18$, $p < 0.001$) compared to Generic Stim (slope = − 2.8%/day, R = 0.76, $F_{(1,88)} = 14.27$, $p < 0.001$) measured over 1000 successive trials across several daily sessions after stimulation was terminated [Fig. 4(a)]. The cumulative facilitation in performance on nonstimulated trials in the above sessions as a function of increased individualized MIMO Stim trials was associated with corresponding improvement in DNMS delay curves shown

NIH-PA Author Manuscript

NIH-PA Author Manuscript

NIH-PA Author Manuscript

in Fig. 4(b), (Trl 180, 240, MIMO Stim $F_{(10,476)} = 5.72$, $p < 0.001$). These changes on nonstimulated trials were accompanied by a corresponding upward shift in mean single trial SR *code strength* (Fig. 2) in the same animals (Fig. 4(b), Trl 180, 240, $X^2_{(30)}=67.2$, $p < 0.001$). In addition, the gradual decline in performance following cessation of individualized MIMO stimulation procedures was accompanied by a delay-dependent decrease in performance ($F_{(10,476)} = 4.23$, $p < 0.001$) as well as a gradual decline in single-trial SR code strength ($X^2_{(30)}=54.6$, $p < 0.01$), as shown in Fig. 4 (Trl 800). These same phasic changes were duplicated, but to a lesser degree, for animals that received Generic Stim Fig. 4, Generic Stim, Trl 180, 240, 800) with the facilitatory effects dissipating more rapidly than individualized MIMO stim ($F_{(10,476)} = 2.53$, $p < 0.01$, Trl 800) after cessation of stimulation trials.

The results depicted in Fig. 4 demonstrate that MIMO model derived stimulation effectively changed normal hippocampal operation such that SR encoding on all trials was facilitated as a direct function of the number of *strong* SR code stimulation exposures (240–400 trials), and that this effect persisted for 800 trials after MIMO stimulation was no longer delivered. These findings confirm the fact that 1) the actual presence of electrical stimulation on a given trial was not required for facilitation of performance after a series of stimulation trials, and 2) the changes detected by the MIMO model that correspond to effective performance across more difficult long delay trials, were provoked to occur naturally in hippocampal ensembles and in parallel with the cumulative increases in performance following repeated exposure to stimulation patterns that were determined by the same process.

4) Neuronal Basis of Hippocampal “Strong Code” Firing Patterns

MIMO model predictions were tested by assessing the relation to performance of the DNMS task, as shown in Figs. 3 and 4. MIMO model derived mean (generic) firing patterns averaged across several animals ($n = 19$) associated with successful performance (*strong* SR codes), or with errors (*weak* SR codes) on trials in the same sessions, are shown in Fig. 5(a) and (b), respectively. Fig. 5(c) shows the relationship of these two types of firing patterns to ensembles recorded in different animals in terms of the correlation of patterns in individual animals (each bar) to the overall mean pattern for each SR. The consistency of correlations ($r = 0.4$ to 0.6) between each animal’s individual MIMO-derived CA1 pattern for Left and Right strong SR codes and the generic CA1 Left and Right strong codes averaged across animals ($n = 20$) shown in Fig. 5(c) indicates that 16%–36% (i.e.$r^2 = 0.16$ to 0.36) of spikes in the mean generic patterns occurred on the same neuron channel and at the same temporal position as in the individual MIMO-derived patterns. This is significantly above the chance correlation ($r = 0.29$, $r^2 = 0.08$) obtained when individual CA1 ensemble spike patterns were randomized, averaged, then correlated to the mean. Fig. 5(d) shows the possible basis for this similarity in terms of prior characterizations and classifications of individual CA1 and CA3 cell firing characteristics in the same DNMS task [22], [27], [33], [35]. The perievent histograms characterize different cell types that show firing correlates to (i.e., encode) specific features of the DNMS task (i.e., lever position, phase of task, and/or conjunctions of both). Although ensemble cell firing is distributed across all task-relevant events, The most complex type firing involves the hierarchical combining of these properties in some neurons, termed Trial-Type cells, that respond only to inputs from what appear to be pairs of conjunctive cells to reconstruct (i.e., encode) particular features which define a type of trial. In this context Trial-Type cells fire only on left SRs and right NRs (Fig. 5(d), lower right) i.e., both behavioral events that define *only one type* of DNMS trial and not anything related to the other. It is important to note that recently it was discovered [22], [27] that this natural encoding feature accounts for a large portion of the differentiation of MIMO patterns into *strong* codes that are present on successful DNMS trials. The MIMO model therefore can

NIH-PA Author Manuscript

NIH-PA Author Manuscript

NIH-PA Author Manuscript

selectively filter occasions in which large numbers of CA1 and CA3 Trial-Type cells fire synchronously on the same. Strong code trial, as shown in Fig. 5(e)

IV. Discussion

The results presented here provide additional evidence to support prior demonstrations [26] that a device employing a nonlinear MIMO model to extract hippocampal ensemble firing patterns online during a delayed memory task can, not only enhance and repair memory but if necessary, also, after repeated exposure, change how the hippocampus alone encodes events to facilitate retrieval and enhance performance. As demonstrated here, the effectiveness of the MIMO derived electrical stimulation patterns delivered to the same hippocampal locations in which they occur during similar task demands (Figs. 3–5) establishes the functional significance of MIMO model extracted SR codes. Although other recent investigations have reported relationships between multineuron firing in cortical ensembles and distinct behavioral events [11], [29], [43], [49]–[57], few have attempted, as performed here, to directly substitute electrical stimulation for behaviorally correlated neuron discharges from the same anatomic loci [58]–[62]. Also unlike other forms of effective brain stimulation [58], [63], [64], the beneficial effects of MIMO derived stimulation requires that the stimulation pulses be delivered in the identical spatio-temporal firing patterns as recorded from the same neural ensembles [14], [23], [24], [60].

The results presented here have taken this analysis to its final level by showing that the "strengths" of SR codes are related directly to the specificity of the lever position that is being encoded and that deviation from this firing pattern specificity is related to a proportional "mixing" of codes between the two lever positions as shown in Fig. 2. The fact that this mixing tendency is proportionately vulnerable to the duration of the intervening delay makes this the primary determinant of successful performance since "strong SR codes" produce maximum success at all delays and "weak SR codes" resemble strong codes for the opposite lever (Fig. 2) and hence are at risk for error at all delays. From these two extremes it is possible to derive measures of code strength from trial specific ensemble firing patterns subjected to MIMO coefficient adjustment and therefore provide an explanation for decreased performance as a function of duration of delay because of the transitional gradients expressed in patterns with different code strengths corresponding to trials with increasing delays. It is clear from Fig. 2 that ensemble codes with intermediate strength between strong and weak codes show a proportionate vulnerability to delay duration strictly as a function of how similar the patterns are to the either the strong code which insures maximal performance at all delays, and weak codes which produce near chance performance on trials > 16 s where hippocampus is required to perform the task [20], [31], [37]. The direct test of this requirement in recent studies showed that the beneficial effect of MIMO stimulation was not present if: 1) stimulation patterns were the same intensities but the SR code was altered by "scrambling" the MIMO derived coefficients across electrode locations and temporal sequences, 2) the exact same effective patterns were delivered at different times during the trial than the SR, and 3) SR code stimulation patterns for each lever were reversed [22], [26]. Randomizing the coefficients of the MIMO model strong code pattern produced a change in the spatiotemporal pattern which when delivered as "scrambled" stimulation no longer facilitated performance and mimicked firing that occurred on trials with intermediate codes where fully developed strong or weak codes were not present [Normal Codes, Fig. 2(b)].

The above intricate analyses make it obvious that the effectiveness of the stimulation patterns cannot be attributed to subjective influences such as acting as a cue to the animal for correct responding for several reasons; 1) the stimulation patterns differ for each lever position which means that if the animal were utilizing the mere presence of stimulation on

NIH-PA Author Manuscript

NIH-PA Author Manuscript

NIH-PA Author Manuscript

certain trials to perform better than nonstimulation trials, it would also have to be capable of discriminating the individual patterns of stimulation for each lever *independent* of the lever position which is very unlikely, also 2) since the stimulation is delivered only at the time of the SR, retrieval of the specific stim pattern as a cue together with lever position (left or right) would also be required at the time of the NR, 10–30 s later, which is unlikely, 3) stimulation patterns in addition to being different for each lever position are delivered to CA1 cells in both hemispheres, therefore it is not possible for differential unilateral activation to provide a cue from the stimulation either, finally and perhaps most relevant to this alternative explanation for the effectiveness of the stimulation is the fact that as shown in Fig. 4, 4) performance on *nonstimulation trials* was systematically and differentially facilitated as a function of the number and type of MIMO stimulation trials previously experienced, which makes it impossible for conditioning to stimulation-related "cues" to have been the basis for improved performance in the DNMS task.

Another cohesive factor in the results reported here that prevents alternative interpretations was that MIMO model derived stimulation was effective because it reflected the predicted *strong* SR code ensemble firing pattern in which performance could be enhanced by its utilization in the closed loop paradigm [22], [26]. In this case enhancing performance by linking the detection of strong codes to trials in which task delays could be lengthened showed that 1) the patterns were generated online coincident with the occurrence of neural events that required encoding and 2) when such "strong" SR codes did occur they were sufficient to survive delays longer than the animal had experienced previously but were still delay-dependent in the same manner as weaker SR codes which were at risk for error [22], [26]. This is also consistent with the fact that the "read out" of the MIMO model derived codes reflect a natural encoding process in hippocampus where behaviorally relevant features of the DNMS task are hierarchically demarcated into the distributed functional cell types [FCTs, Fig. 5(d) and (e)] that have been shown extensively in prior studies [16], [27], [33], [35], [65]. The fact that *strong* SR codes occurred only on trials with a high percentage of synchronously firing appropriate Trial-Type cells [Fig. 5(e)], provides a biological basis for the success of the MIMO model stimulation in facilitating performance since prior investigations have shown that such hierarchical encoding and distribution of task information amongst hippocampal cell types occurs only after delays are introduced in the DNMS training regimen [33], [35], [66].

An important new feature of MIMO model stimulation shown in Fig. 4 appears to exploit the well-known long-term plasticity of hippocampal synaptic circuitry [48], [52], [67]–[70] via cumulative effects after repetitive *strong* SR code stimulation trials exhibited by improved performance on nonstimulation trials progressively over time in the same behavioral sessions. The subsequent gradual decline in enhanced performance over days on nonstimulated trials after stimulation was terminated, suggests that the changes provoked in hippocampal plasticity underlying effective SR encoding were likely due to synaptic degradation in the absence of continued potentiation from MIMO stimulation [71], [72]. The fact that the frequency of spontaneously generated *strong* SR codes increased on nonstimulated trials during cumulative MIMO stimulation trials and decreased to near prestimulation levels after stimulation was terminated (Fig. 4) is also supportive of synaptic mechanisms being altered. This feature indicates that such patterned stimulation may have tapped directly into factors known to control long term potentiation (LTP) of hippocampal synaptic processes such as, 1) frequency of stimulus pulses within the train, 2) number of times pulse trains are delivered, and because of the nonlinear nature of MIMO model derivations [23], [39], [73]–[75], 3) the polarization status of postsynaptic cell membrane at the time of convergent presynaptic inputs [71], [72], [76], [77]. If synaptic potentiation were being provoked by cumulative MIMO model stimulation a possible direct consequence would be an enhanced tendency for subclasses of appropriate Trial-Type cells to fire

NIH-PA Author Manuscript

NIH-PA Author Manuscript

NIH-PA Author Manuscript

synchronously on nearly every trial, thereby producing nearly automatic encoding and accurate performance as shown when such firing occurred spontaneously (Fig. 2). The above results clearly illustrate the difference between individualized MIMO stimulation patterns derived online from the CA3 region and "Generic Stim" patterns averaged across large numbers of similarly trained and tested animals (Fig. 4). However, the virtual standardization of the DNMS recording circumstances across animals made possible the application of the MIMO model as universal hippocampal prosthesis since in this context it was possible to employ Generic stimulation patterns without preassessment and derivation of individual stimulation parameters online. We have reported recently that this approach can be used to replace hippocampal function when ensemble firing no longer produces task-related *strong* SR codes due to pharmacological blockade of glutamatergic transmission [26].

This is also consistent with the fact that the "read out" of the MIMO model derived codes reflect a natural encoding process in hippocampus where relevant features of the DNMS task are hierarchically demarcated into the distributed functional cell types [FCTs, Fig. 5(d) and (e)] that have been shown extensively in prior studies [16], [27], [33], [35], [65]. The fact that *strong* SR codes occurred only on trials with a high percentage of synchronously firing appropriate Trial-Type cells [Fig. 5(e)], provides a biological basis for the success of the MIMO model stimulation in facilitating performance since prior investigations have shown that such hierarchical encoding and distribution of task information amongst hippocampal cell types occurs only after delays are introduced in the DNMS training regimen [33], [35], [66]. Finally, the fact that MIMO model patterns of electrical brain stimulation can repair and/or enhance cognitive efficiency suggests that cortical prostheses of this nature could be implemented in a variety of brain regions if applied in a manner consistent with the ensemble information processing they are intended to replace [29], [30], [50], [78]–[81].

Acknowledgments

This work was supported by The Defense Advanced Research Projects Agency (Contract N66601-09-C-2080 to S. A. Deadwyler and N66601-09-C-2081 to T. W. Berger). The views, opinions, and/or findings contained in this paper are those of the author and should not be interpreted as representing the official views or policies, either expressed or implied, of the Defense Advanced Research Projects Agency or the Department of Defense. This work was also supported in part by grants National Science Foundation (NSF) EEC-0310723 to University of Southern California (USC) (T. W. Berger), National Institutes of Health/National Institute of Biomedical Imaging and Bioengineering (NIH/NIBIB) under Grant P41-EB001978 to the Biomedical Simulations Resource at USC (V. Z. Marmarelis and T.W. Berger), and NIH R01DA07625 (S. A. Deadwyler).

The authors would like to thank P. Huettl (University of Kentucky), and C. Collins, V. Collins, C. Dyson, G. McLeod, and M. Moran (WFSM) for their contributions.

References

1. Eichenbaum H, Fortin NJ. The neurobiology of memory based predictions. Philos. Trans. R. Soc. Lond B Biol. Sci. 2009; vol. 364:1183–1191. [PubMed: 19527999]
2. Davachi L. Item, context and relational episodic encoding in humans. Curr. Opin. Neurobiol. 2006; vol. 16:693–700. [PubMed: 17097284]
3. Gold JJ, Smith CN, Bayley PJ, Shrager Y, Brewer JB, Stark CE, Hopkins RO, Squire LR. Item memory, source memory, and the medial temporal lobe: Concordant findings from fMRI and memory-impaired patients. Proc. Natl. Acad. Sci. 2006; vol. 103:9351–9356. [PubMed: 16751272]
4. Eichenbaum H, Yonelinas AP, Ranganath C. The medial temporal lobe and recognition memory. Annu. Rev. Neurosci. 2007; vol. 30:123–152. [PubMed: 17417939]
5. Klausberger T, Somogyi P. Neuronal diversity and temporal dynamics: The unity of hippocampal circuit operations. Science. 2008; vol. 321:53–57. [PubMed: 18599766]

NIH-PA Author Manuscript

NIH-PA Author Manuscript

NIH-PA Author Manuscript

6. Manns JR, Hopkins RO, Reed JM, Kitchener EG, Squire LR. Recognition memory and the human hippocampus. Neuron. 2003; vol. 37:171–180. [PubMed: 12526782]
7. Squire LR, Wixted JT, Clark RE. Recognition memory and the medial temporal lobe: A new perspective. Nat. Rev. Neurosci. 2007; vol. 8:872–883. [PubMed: 17948032]
8. Eichenbaum, H.; Cohen, NJ. From Conditioning to Conscious Recollection: Memory Systems of the Brain. New York: Oxford Univ. Press; 2001.
9. Quirk GJ, Muller RU, Kubie JL, Ranck JB Jr. The positional firing properties of medial entorhinal neurons: Description and comparison with hippocampal place cells. J. Neurosci. 1992; vol. 12:1945–1963. [PubMed: 1578279]
10. Ross RS, Slotnick SD. The hippocampus is preferentially associated with memory for spatial context. J. Cogn Neurosci. 2008; vol. 20:432–446. [PubMed: 18004952]
11. Rutishauser U, Mamelak AN, Schuman EM. Single-trial learning of novel stimuli by individual neurons of the human hippocampus-amygdala complex. Neuron. 2006; vol. 49:805–813. [PubMed: 16543129]
12. Wais PE, Wixted JT, Hopkins RO, Squire LR. The hippocampus supports both the recollection and the familiarity components of recognition memory. Neuron. 2006; vol. 49:459–466. [PubMed: 16446148]
13. Winters BD, Bussey TJ. Transient inactivation of perirhinal cortex disrupts encoding, retrieval, and consolidation of object recognition memory. J. Neurosci. 2005; vol. 25:52–61. [PubMed: 15634766]
14. Song D, Chan RH, Marmarelis VZ, Hampson RE, Deadwyler SA, Berger TW. Nonlinear dynamic modeling of spike train transformations for hippocampal-cortical prostheses. IEEE Trans. Biomed. Eng. 2007 Jun.vol. 54(no. 6):1053–1066. [PubMed: 17554824]
15. Berger TW, Ahuja A, Courellis SH, Deadwyler SA, Erinjippurath G, Gerhardt GA, Gholmieh G, Granacki JJ, Hampson R, Hsaio MC, LaCoss J, Marmarelis VZ, Nasiatka P, Srinivasan V, Song D, Tanguay AR, Wills J. Restoring lost cognitive function. IEEE Eng. Med. Biol. Mag. 2005 Sep-Oct;vol. 24(no. 5):30–44. [PubMed: 16248115]
16. Hampson, RE.; Simeral, JD.; Deadwyler, SA. Cognitive processes in replacement brain parts: A code for all reasons. In: Berger, TW.; Glanzman, DL., editors. Toward Replacement Parts for the Brain. Implantable Biomimetic Electronics as Neural Prosthesis. Cambridge, MA: MIT Press; 2005. p. 111-128.
17. Marmarelis VZ, Orme ME. Modeling of neural systems by use of neuronal modes. IEEE Trans. Biomed. Eng. 1993 Nov.vol. 40(no. 11):1149–1158. [PubMed: 8307599]
18. Truccolo W, Eden UT, Fellows MR, Donoghue JP, Brown EN. A point process framework for relating neural spiking activity to spiking history, neural ensemble, and extrinsic covariate effects. J. Neurophysiol. 2005; vol. 93:1074–1089. [PubMed: 15356183]
19. Song D, Chan RH, Marmarelis VZ, Hampson RE, Deadwyler SA, Berger TW. Nonlinear modeling of neural population dynamics for hippocampal prostheses. Neural Netw. 2009; vol. 22:1340–1351. [PubMed: 19501484]
20. Deadwyler SA, Hampson RE. Temporal coupling between subicular and hippocampal neurons underlies retention of trial-specific events. Behav. Brain Res. 2006; vol. 174:272–280. [PubMed: 16876266]
21. Deadwyler SA, Bunn T, Hampson RE. Hippocampal ensemble activity during spatial delayed-nonmatch-to-sample performance in rats. J. Neurosci. 1996; vol. 16:354–372. [PubMed: 8613802]
22. Hampson, RE.; Simeral, JD.; Berger, TW.; Song, D.; Chan, RHM.; Deadwyler, SA. Cognitively relevant recording in hippocampus: Beneficial feedback of ensemble codes in a closed loop paradigm. In: Vertes, RP.; Stackman, RW., editors. Electrophysiological Recording Techniques. New York: Humana; 2011. p. 215-240.
23. Zanos TP, Courellis SH, Berger TW, Hampson RE, Deadwyler SA, Marmarelis VZ. Nonlinear modeling of causal interrelationships in neuronal ensembles. IEEE Trans. Neural Syst. Rehabil. Eng. 2008 Aug; vol. 16(no. 4):336–352. [PubMed: 18701382]
24. Song D, Chan RH, Marmarelis VZ, Hampson RE, Deadwyler SA, Berger TW. Statistical selection of multiple-input multiple-output nonlinear dynamic models of spike train transformation. Proc. IEEE Eng Med. Biol. Soc. Conf. 2007; vol. 2007:4727–4730.

NIH-PA Author Manuscript

NIH-PA Author Manuscript

NIH-PA Author Manuscript

25. Marmarelis, VZ. Nonlinear Dynamic Modeling of Physiological Systems. Hoboken, NJ: Wiley-IEEE Press; 2004.
26. Berger TW, Hampson RE, Song D, Goonawardena A, Marmarelis VZ, Deadwyler SA. A cortical neural prosthesis for restoring and enhancing memory. J. Neural Eng. 2011; vol. 8 046017.
27. Hampson, RE.; Simeral, JD.; Deadwyler, SA. Neural population recording in behaving animals: Constituents of the neural code for behavior. In: Holscher, C.; Munk, MH., editors. Neural Population Encoding. Cambridge, U.K.: Cambridge Univ. Press; 2008. p. 74-94.
28. Chapin JK. Using multi-neuron population recordings for neural prosthetics. Nat. Neurosci. 2004; vol. 7:452–455. [PubMed: 15114357]
29. Schwartz AB, Moran DW, Reina GA. Differential representation of perception and action in the frontal cortex. Science. 2004; vol. 303:380–383. [PubMed: 14726593]
30. Wessberg J, Stambaugh CR, Kralik JD, Beck PD, Laubach M, Chapin JK, Kim J, Biggs SJ, Srinivasan MA, Nicolelis MA. Real-time prediction of hand trajectory by ensembles of cortical neurons in primates. Nature. 2000; vol. 408:361–365. [PubMed: 11099043]
31. Deadwyler SA, Hampson RE. Differential but complementary mnemonic functions of the hippocampus and subiculum. Neuron. 2004; vol. 42:465–476. [PubMed: 15134642]
32. Hampson RE, Deadwyler SA. Temporal firing characteristics and the strategic role of subicular neurons in short-term memory. Hippocampus. 2003; vol. 13:529–541. [PubMed: 12836920]
33. Hampson RE, Simeral JD, Deadwyler SA. Distribution of spatial and nonspatial information in dorsal hippocampus. Nature. 1999; vol. 402:610–614. [PubMed: 10604466]
34. Paxinos, G.; Watson, C. The Rat Brain in Stereotaxic Coordinates. 3rd ed.. San Diego, CA: Academic; 1997.
35. Goonawardena AV, Robinson L, Riedel G, Hampson RE. Recruitment of hippocampal neurons to encode behavioral events in the rat: Alterations in cognitive demand and cannabinoid exposure. Hippocampus. 2010; vol. 20:1083–1094. [PubMed: 19771586]
36. Deadwyler SA, Goonawardena AV, Hampson RE. Short-term memory is modulated by the spontaneous release of endocannabinoids: Evidence from hippocampal population codes. Behav. Pharmacol. 2007; vol. 18(no. 5–6):571–580. [PubMed: 17762525]
37. Simeral, JD.; Hampson, RE.; Deadwyler, SA. Behaviorally relevant neural codes in hippocampal ensembles: Detection on single trials. In: Baudry, M.; Bi, X.; Schreiber, S., editors. Synaptic Plasticity: From Basic Mechanisms to Clinical Applications. Cambridge, MA: MIT Press; 2005. p. 459-476.
38. Chan RH, Song D, Goonawardena AV, Bough S, Sesay J, Hampson RE, Deadwyler SA, Berger TW. Changes of hippocampalCA3-CA1 population nonlinear dynamics across different training sessions in rats performing a memory-dependent task. Proc. IEEE Eng Med. Biol. Soc. Conf. 2010; vol. 2010:5464–5467.
39. Zanos TP, Hampson RE, Deadwyler SE, Berger TW, Marmarelis VZ. Boolean modeling of neural systems with point-process inputs and outputs. Part II: Application to the rat hippocampus. Ann. Biomed. Eng. 2009; vol. 37:1668–1682. [PubMed: 19499341]
40. Zanos TP, Hampson RE, Deadwyler SA, Berger TW, Marmarelis VZ. Functional connectivity through nonlinear modeling: An application to the rat hippocampus. Proc. IEEE Eng Med. Biol. Soc. Conf. 2008; vol. 2008:5522–5525.
41. Song D, Chan RH, Marmarelis VZ, Hampson RE, Deadwyler SA, Berger TW. Sparse generalized Laguerre-Volterra model of neural population dynamics. Proc. IEEE Eng. Med. Biol. Soc. Conf. 2009; vol. 2009:4555–4558.
42. Song D, Chan RHM, Marmarelis VZ, Hampson RE, Deadwyler SA, Berger TW. Generalized Volterra Model for Spike Train Transformations in the Hippocampus. 2008; vol. 1:4555–4558.
43. Brown EN, Barbieri R, Ventura V, Kass RE, Frank LM. The time-rescaling theorem and its application to neural spike train data analysis. Neural Comput. 2002; vol. 14:325–346. [PubMed: 11802915]
44. Deadwyler SA, Hampson RE. Endocannabinoids modulate encoding of sequential memory in the rat hippocampus. Psychopharmacology (Berl). 2008; vol. 198:577–586. [PubMed: 18210094]

NIH-PA Author Manuscript

NIH-PA Author Manuscript

NIH-PA Author Manuscript

45. Hampson RE, Jarrard LE, Deadwyler SA. Effects of ibotenate hippocampal and extrahippocampal destruction on delayed-match and -nonmatch-to-sample behavior in rats. J. Neurosci. 1999; vol. 19:1492–1507. [PubMed: 9952425]
46. Deadwyler, SA.; Hampson, RE. The significance of neural ensemble codes during behavior and cognition. In: Cowan, WM.; Shooter, EM.; Stevens, CF.; Thompson, RF., editors. Annual Review of Neuroscience. Vol. vol. 20. Palo Alto, CA: Annual Reviews; 1997. p. 217-244.
47. Deadwyler SA, Hampson RE. Ensemble activity and behavior: What's the code? Science. 1995; vol. 270:1316–1318. [PubMed: 7481817]
48. Morris RG. Long-term potentiation and memory. Philos. Trans. R. Soc. Lond. B Biol. Sci. 2003; vol. 358:643–647. [PubMed: 12740109]
49. Diba K, Buzsaki G. Hippocampal network dynamics constrain the time lag between pyramidal cells across modified environments. J. Neurosci. 2008; vol. 28:13448–13456. [PubMed: 19074018]
50. Hochberg LR, Serruya MD, Friehs GM, Mukand JA, Saleh M, Caplan AH, Branner A, Chen D, Penn RD, Donoghue JP. Neuronal ensemble control of prosthetic devices by a human with tetraplegia. Nature. 2006; vol. 442:164–171. [PubMed: 16838014]
51. Jensen O, Lisman JE. Hippocampal sequence-encoding driven by a cortical multi-item working memory buffer. Trends Neurosci. 2005; vol. 28:67–72. [PubMed: 15667928]
52. Klyachko VA, Stevens CF. Excitatory and feed-forward inhibitory hippocampal synapses work synergistically as an adaptive filter of natural spike trains. PLoS. Biol. 2006; vol. 4:E207. [PubMed: 16774451]
53. Lebedev MA, Messinger A, Kralik JD, Wise SP. Representation of attended versus remembered locations in prefrontal cortex. PLoS. Biol. 2004; vol. 2:E365. [PubMed: 15510225]
54. Moser EI, Kropff E, Moser MB. Place cells, grid cells, and the brain's spatial representation system. Annu. Rev. Neurosci. 2008; vol. 31:69–89. [PubMed: 18284371]
55. Pastalkova E, Itskov V, Amarasingham A, Buzsaki G. Internally generated cell assembly sequences in the rat hippocampus. Science. 2008; vol. 321:1322–1327. [PubMed: 18772431]
56. Ross RS, Eichenbaum H. Dynamics of hippocampal and cortical activation during consolidation of a nonspatial memory. J. Neurosci. 2006; vol. 26:4852–4859. [PubMed: 16672659]
57. Smith NJ, Narayanan NS, Laubach M. Past performance is indicative of future returns. Neuron. 2009; vol. 63:146–148. [PubMed: 19640473]
58. Canals S, Beyerlein M, Murayama Y, Logothetis NK. Electric stimulation fMRI of the perforant pathway to the rat hippocampus. Magn. Reson. Imag. 2008; vol. 26:978–986.
59. Canals S, Beyerlein M, Merkle H, Logothetis NK. Functional MRI evidence for LTP-induced neural network reorganization. Curr. Biol. 2009; vol. 19:398–403. [PubMed: 19230667]
60. Moritz CT, Perlmutter SI, Fetz EE. Direct control of paralysed muscles by cortical neurons. Nature. 2008; vol. 456:639–642. [PubMed: 18923392]
61. Murphey DK, Maunsell JH. Electrical microstimulation thresholds for behavioral detection and saccades in monkey frontal eye fields. Proc. Nat. Acad. Sci. USA. 2008; vol. 105:7315–7320. [PubMed: 18477698]
62. Murphey DK, Maunsell JH, Beauchamp MS, Yoshor D. Perceiving electrical stimulation of identified human visual areas. Proc. Nat. Acad. Sci. USA. 2009; vol. 106:5389–5393. [PubMed: 19276119]
63. Dulay MF, Murphey Sun DK, Sun P, David YB, Maunsell JH, Beauchamp MS, Yoshor D. Computer-controlled electrical stimulation for quantitative mapping of human cortical function. J. Neurosurg. 2009; vol. 110:1300–1303. [PubMed: 19061348]
64. Lega BC, Halpern CH, Jaggi JL, Baltuch GH. Deep brain stimulation in the treatment of refractory epilepsy: Update on current data and future directions. Neurobiol. Dis. 2009
65. Hampson, RE.; Deadwyler, SA. Differential information processing by hippocampal and subicular neurons. In: Witter, MP., editor. The Parahippocampal Region: Special Supplement to the Annals of the New York Academy of Sciences. New York: NY Acad. Sci.; 2000.
66. Chan RH, Song D, Goonawardena AV, Bough S, Sesay J, Hampson RE, Deadwyler SA, Berger TW. Changes of hippocampal Ca3-Ca1 population nonlinear dynamics across different training

NIH-PA Author Manuscript

NIH-PA Author Manuscript

NIH-PA Author Manuscript

sessions in rats performing a memory-dependent task. Proc. IEEE Eng Med. Biol. Soc. Conf. 2010; vol. 2010:5464–5467.

67. Nader K, Hardt O. A single standard for memory: The case for reconsolidation. Nat. Rev. Neurosci. 2009; vol. 10:224–234. [PubMed: 19229241]
68. Wang XB, Bozdagi O, Nikitczuk JS, Zhai ZW, Zhou Q, Huntley GW. Extracellular proteolysis by matrix metalloproteinase-9 drives dendritic spine enlargement and long-term potentiation coordinately. Proc. Nat. Acad. Sci. USA. 2008; vol. 105:19520–19525. [PubMed: 19047646]
69. Fedulov V, Rex CS, Simmons DA, Palmer L, Gall CM, Lynch G. Evidence that long-term potentiation occurs within individual hippocampal synapses during learning. J. Neurosci. 2007; vol. 27:8031–8039. [PubMed: 17652593]
70. Abraham WC, Logan B, Greenwood JM, Dragunow M. Induction and experience-dependent consolidation of stable long-term potentiation lasting months in the hippocampus. J. Neurosci. 2002; vol. 22:9626–9634. [PubMed: 12417688]
71. Kelly MT, Yao Y, Sondhi R, Sacktor TC. Actin polymerization regulates the synthesis of PKMzeta in LTP. Neuropharmacology. 2007; vol. 52:41–45. [PubMed: 16914172]
72. Lynch G, Rex CS, Chen LY, Gall CM. The substrates of memory: defects, treatments, and enhancement. Eur. J. Pharmacol. 2008; vol. 585:2–13. [PubMed: 18374328]
73. Marmarelis VZ, Zanos TP, Berger TW. Boolean modeling of neural systems with point-process inputs and outputs. Part I: Theory and simulations. Ann. Biomed. Eng. 2009; vol. 37:1654–1667. [PubMed: 19517238]
74. Song D, Marmarelis VZ, Berger TW. Parametric and nonparametric modeling of short-term synaptic plasticity. Part I: Computational study. J. Comput. Neurosci. 2009; vol. 26:1–19. [PubMed: 18506609]
75. Song D, Wang Z, Marmarelis VZ, Berger TW. Parametric and non-parametric modeling of short-term synaptic plasticity. Part II: Experimental study. J. Comput. Neurosci. 2009; vol. 26:21–37. [PubMed: 18504530]
76. Wu LJ, Ren M, Wang H, Kim SS, Cao X, Zhuo M. Neurabin contributes to hippocampal long-term potentiation and contextual fear memory. PLoS. One. 2008; vol. 3:E1407. [PubMed: 18183288]
77. Lin B, Kramar EA, Bi X, Brucher FA, Gall CM, Lynch G. Theta stimulation polymerizes actin in dendritic spines of hippocampus. J. Neurosci. 2005; vol. 25:2062–2069. [PubMed: 15728846]
78. Watson DJ, Herbert MR, Stanton ME. Nmda receptor involvement in spatial delayed alternation in developing rats. Behav. Neurosci. 2009; vol. 123:44–53. [PubMed: 19170429]
79. Mavoori J, Jackson A, Diorio C, Fetz E. An autonomous implantable computer for neural recording and stimulation in unrestrained primates. J. Neurosci. Methods. 2005; vol. 148:71–77. [PubMed: 16102841]
80. Jackson A, Mavoori J, Fetz EE. Long-term motor cortex plasticity induced by an electronic neural implant. Nature. 2006; vol. 444:56–60. [PubMed: 17057705]
81. Jarosiewicz B, Chase SM, Fraser GW, Velliste M, Kass RE, Schwartz AB. Functional network reorganization during learning in a brain-computer interface paradigm. Proc. Nat. Acad. Sci. 2008; vol. 105:19486–19491. [PubMed: 19047633]

Biographies

Robert E. Hampson (M’09) received the Ph.D. degree in physiology from Wake Forest University, Winston-Salem, NC, in 1988.

He is an Associate Professor at the Department of Physiology and Pharmacology, Wake Forest University School of Medicine, Winston-Salem, NC. His main interests are in

NIH-PA Author Manuscript

NIH-PA Author Manuscript

NIH-PA Author Manuscript

learning and memory: in particular deciphering the neural code utilized by the hippocampus and other related structures to encode behavioral events and cognitive decisions. He has published extensively in the areas of cannabinoid effects on behavior and electrophysiology, and the correlation of behavior with multineuron activity patterns, particularly applying linear discriminant analysis to neural data to decipher population encoding and representation.

Dong Song (S'02–M'04) received the B.S. degree in biophysics from the University of Science and Technology of China, Hefei, China, in 1994, and the Ph.D. degree in biomedical engineering from the University of Southern California, Los Angeles, in 2003.

He is a Research Assistant Professor in the Department of Biomedical Engineering, University of Southern California, Los Angeles. His research interests include nonlinear systems analysis, cortical neural prosthesis, electrophysiology of the hippocampus, and development of novel modeling techniques incorporating both parametric and nonparametric modeling methods.

Dr. Song is a member of the American Statistical Association, the Biomedical Engineering Society, and the Society for Neuroscience.

Rosa H. M. Chan (S'08) received the B.Eng. (1st Hon.) degree in automation and computer-aided engineering from the Chinese University of Hong Kong, in 2003. She was later awarded the Croucher Scholarship and Sir Edward Youde Memorial Fellowship for Overseas Studies in 2004. She received M.S. degrees in biomedical engineering, electrical engineering, and aerospace engineering, and the Ph.D. degree in biomedical engineering, in 2011, all from the University of Southern California, Los Angeles.

She is currently an Assistant Professor in the Department of Electronic Engineering at City University of Hong Kong. Her research interests include computational neuroscience and development of neural prosthesis.

Andrew J. Sweatt received the B.A. degree in natural sciences from the Johns Hopkins University, Baltimore, MD, in 1974, the M.S. degree in biological oceanography from the University of Rhode Island, Kingston, in 1978, and the Ph.D. degree in zoology from Duke University, Durham NC, in 1983.

NIH-PA Author Manuscript

NIH-PA Author Manuscript

NIH-PA Author Manuscript

He is an Assistant Professor in the Department of Physiology and Pharmacology, Wake Forest University School of Medicine, Winston-Salem, NC. His published work has been in the areas of retinal, corneal, and neural cell biology, with recent focus on brain amino acid metabolism. Current interests are in cellular mechanisms underlying the role of the hippocampus in short-term memory.

Mitchell R. Riley received the B.S. degree in athletic training/sports medicine from Appalachian State University, Boone, NC, in 2009. He is currently working toward the Ph.D. degree in neuroscience at Wake Forest University School of Medicine, Winston-Salem, NC.

His research interests include learning, memory, and cognitive decline, with a focus on translational models.

Mr. Riley is a member of the Society for Neuroscience.

Gregory A. Gerhardt received the Ph.D. degree in chemistry from the University of Kansas, in 1983. He received postdoctoral training in pharmacology, neuroscience, and psychiatry at the University of Colorado Health Sciences Center, Denver, from 1983 to 1985.

He is currently a Professor in the Anatomy and Neurobiology, Neurology, and Psychiatry Departments at the University of Kentucky (UK) Chandler Medical Center, Lexington. He is the Director of the Morris K. Udall Parkinson's Disease Research Center of Excellence and Director of the Center for Sensor Technology (CenSeT), both at UK. He is also the Editor-in-Chief, Americas and Australasia, of the *Journal of Neuroscience Methods*. His laboratory develops microelectrode recording methods to study the dynamics of neurotransmitter release in the CNS and to develop neuronal interface devices.

Dae C. Shin (S'81–M'95) received the B.S. and M.S. degrees in electrical engineering from the Seoul National University, Seoul, Korea, in 1982 and 1984, respectively, and both the M.S. and Ph.D. degrees in electrical engineering from the University of Southern California, Los Angeles, in 1988 and 1994, respectively.

NIH-PA Author Manuscript

NIH-PA Author Manuscript

NIH-PA Author Manuscript

His primary research interests are statistical signal processing, linear and nonlinear dynamic modeling of biomedical systems, with special focus on multi-input/multi-output and closed-loop modeling with applications to neural information processing and physiological autoregulation. He retains a research interest in 3-D ultrasound tomography, adaptive signal processing and radar/sonar signal processing. He has published many papers in peer-reviewed journals and conference proceedings.

Vasilis Z. Marmarelis (M'78–F'95) was born in Mytiline, Greece, on November 16, 1949. He received the Diploma in electrical engineering and mechanical engineering from the National Technical University of Athens, Athens, Greece, in 1972, and the M.S. and Ph.D. degrees in engineering science (information science and bioinformation systems) from the California Institute of Technology, Pasadena, in 1973 and 1976, respectively.

He has published more than 100 papers and book chapters in the areas of system modeling and signal analysis.

He is a Fellow of the American Institute for Medical and Biological Engineering.

Theodore W. Berger (SM'05–F'10) received the Ph.D. degree from Harvard University, Cambridge, MA, in 1976. His thesis work received the James McKeen Cattell Award from the New York Academy of Sciences.

He has published over 250 journal articles and book chapters, and is the co-editor of Toward Replacement Parts for the Brain: Implantable Biomimetic Electronics as Neural Prostheses (MIT Press, 2005), as well as the lead co-editor of Brain-Computer Interfaces (Springer, 2008). His research continues to be supported by DARPA, ONR, NSF, NIBIB, and NINDS. Translation of some of His research efforts have led to commercialization efforts through three companies: Safety Dynamics, Inc., Rhenovia Pharma, and Neuralgenix LLC.

Samuel A. Deadwyler (M'09) is a Professor and former Vice Chair (1989–2005) in the Department of Physiology and Pharmacology, Wake Forest University School of Medicine, Winston-Salem, NC, where he has been since 1978. He has published extensively in the area of neural mechanisms of learning and memory. His current research interests include mechanisms of information encoding in hippocampus and frontal cortex also funded by DARPA to design and implement neural prostheses in primate brain.

Dr. Deadwyler has been funded by the National Institutes of Health (NIH) continuously since 1974, recipient of a NIH Senior Research Scientist award from 1987 to 2008, and a MERIT award from 1990 to 2000.

NIH-PA Author Manuscript

NIH-PA Author Manuscript

NIH-PA Author Manuscript

NIH-PA Author Manuscript
NIH-PA Author Manuscript
NIH-PA Author Manuscript

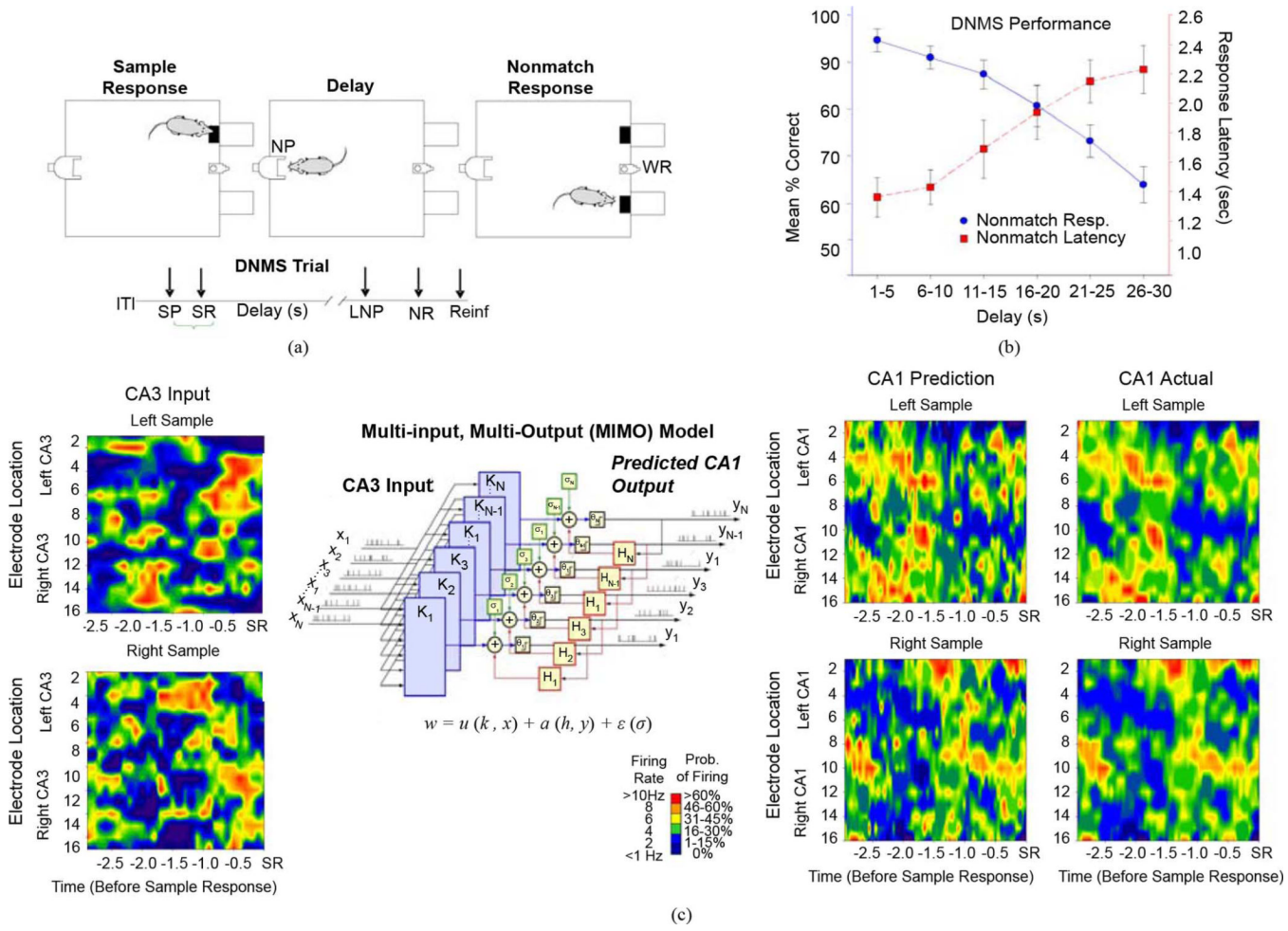

Fig. 1.

DNMS task and associated hippocampal ensemble activity. (a) DNMS trial diagram of SR, Delay, and NR for water reward (WR) Timeline below indicates sequence of phases in the task: intertrial interval (IT); Sample Presentation (SP); Sample response (SR); Delay interval (Delay); last nosepoke (NP) during Delay (LNP); Nonmatch response (NR); Reinforcement (water reward) (Reinf.). (b) DNMS performance for 15 animals. Blue trace indicates mean ± S.E.M. % correct Nonmatch Responses on DNMS trials sorted according to length of delay (in 5 s increments). Red Trace indicates latency to perform the Nonmatch Response on the same trails. (c)MIMO nonlinear model analysis of DNMS generated hippocampal ensemble activity. Left: Color contours depict ensemble firing from 16 CA3 neurons (8 per hemisphere) recorded up to 3.0 s prior to the SR on Left (upper) or Right (lower) DNMS trials. Center: Schematic of MIMO model. CA3 input spike trains $X_1 - X_n$ predict CA1 output spike trains $Y_1 - Y_n$ at right. The input–output relationship between CA3 and CA1 is modeled b parallel MISO nonlinear equations: $w = u(k, x) + a(h, y) + n(\sigma)$, where k indicates the Volterra kernels, σ is a noise term, and H is a feedback term. The MIMO model is constructed of parallel MISO computations expanded with corresponding definitions. Near Right: MIMO predicted CA1 output for Left and Right Sample derived via MIMO model from the CA3 firing input at left. Far Right: Actual CA1 firing corresponding to the MIMO model output. Neuron firing rates spike probability indicated by color scale.

NIH-PA Author Manuscript
NIH-PA Author Manuscript
NIH-PA Author Manuscript

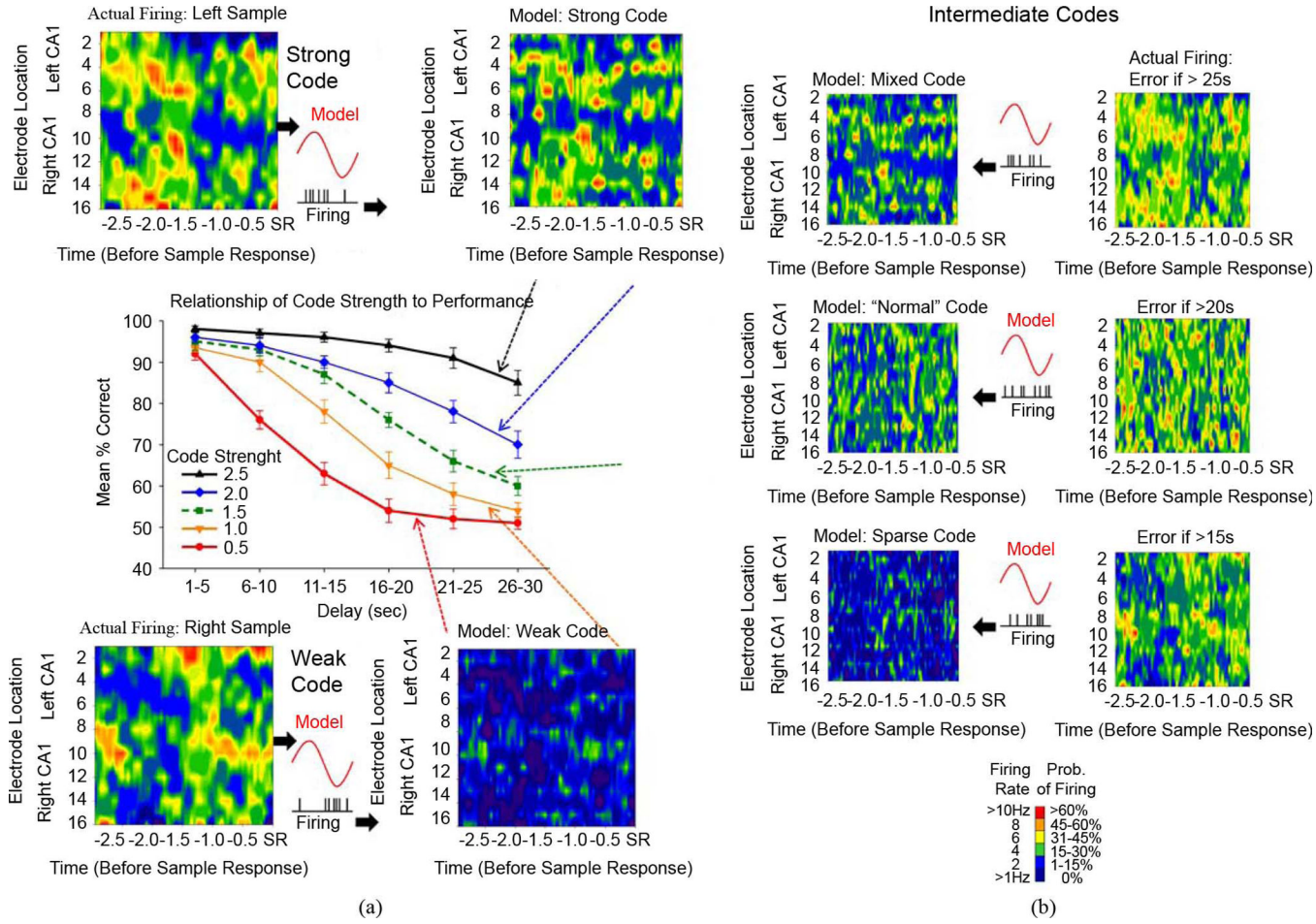

Fig. 2.

DNMS performance level corresponds to strength of SR encoding. (a) Contour Plots illustrate derivation of SR encoding using the MIMO model. Top: CA1 firing in Sample phase of correct Left trials *(Actual Firing)* constitutes a Strong Code. CA3 firing for the same trials, input to the MIMO model, produces the corresponding Strong Code output prediction of CA1 firing. Weighted CA1 firing map *(Model: Strong Code)* is derived from product of CA1 firing with model coefficients as $x_{\text{Left}} \bullet w_{\text{Left}}$, where x_{Left} = Left SR ensemble firing (by neuron and time), and w_{Left} = the MIMO weighting coefficients for correct Left trials. Bottom: CA1 firing corresponding to *opposite* trial (Right Sample) demonstrates lack of correlation between CA1 firing (Actual Firing) and model coefficients which produces low code strength (Model: Weak Code) for the Left Sample. Center: Graph shows DNMS performance on trials with varying strength of SR encoding. Code strength computed as the correlation between CA1 actual firing on DNMS trials and MIMO-predicted Left Correct SR firing (normalized with mean = 0, standard deviation = 1). Colored-coded curves show DNMS performance on trials at different delay durations associated with the respective weighted CA1 firing (dashed arrows); for example, Strong Codes are associated with high level (correct) DNMS performance at all delays (black trace), while Weak Codes are predominantly associated with errors at delays > 10 s (red line). Green dashed trace illustrates "Normal" DNMS performance equivalent to control trace in Fig. 1(b) B: Intermediate Codes: "Mixed," "Normal," and "Sparse" codes result from combination of both correct and incorrect trial firing input to the MIMO model. Each MIMO model output is shown with actual firing representative from single trials with

performance consistent with the behavioral graph for the respective code strength at left. Errors are indicated for delays at each code level. The “Normal” code reflects the MIMO model for trials associated with the behavioral performance associated with 1.5 code strength (Green dashed line) that occurred on normal trials with no strong or weak codes present. Insets: Schematic illustrates correspondence between model coefficients (red curve) and CA1 firing (raster) for each of the SR code conditions.

NIH-PA Author Manuscript
NIH-PA Author Manuscript
NIH-PA Author Manuscript

NIH-PA Author Manuscript
NIH-PA Author Manuscript
NIH-PA Author Manuscript

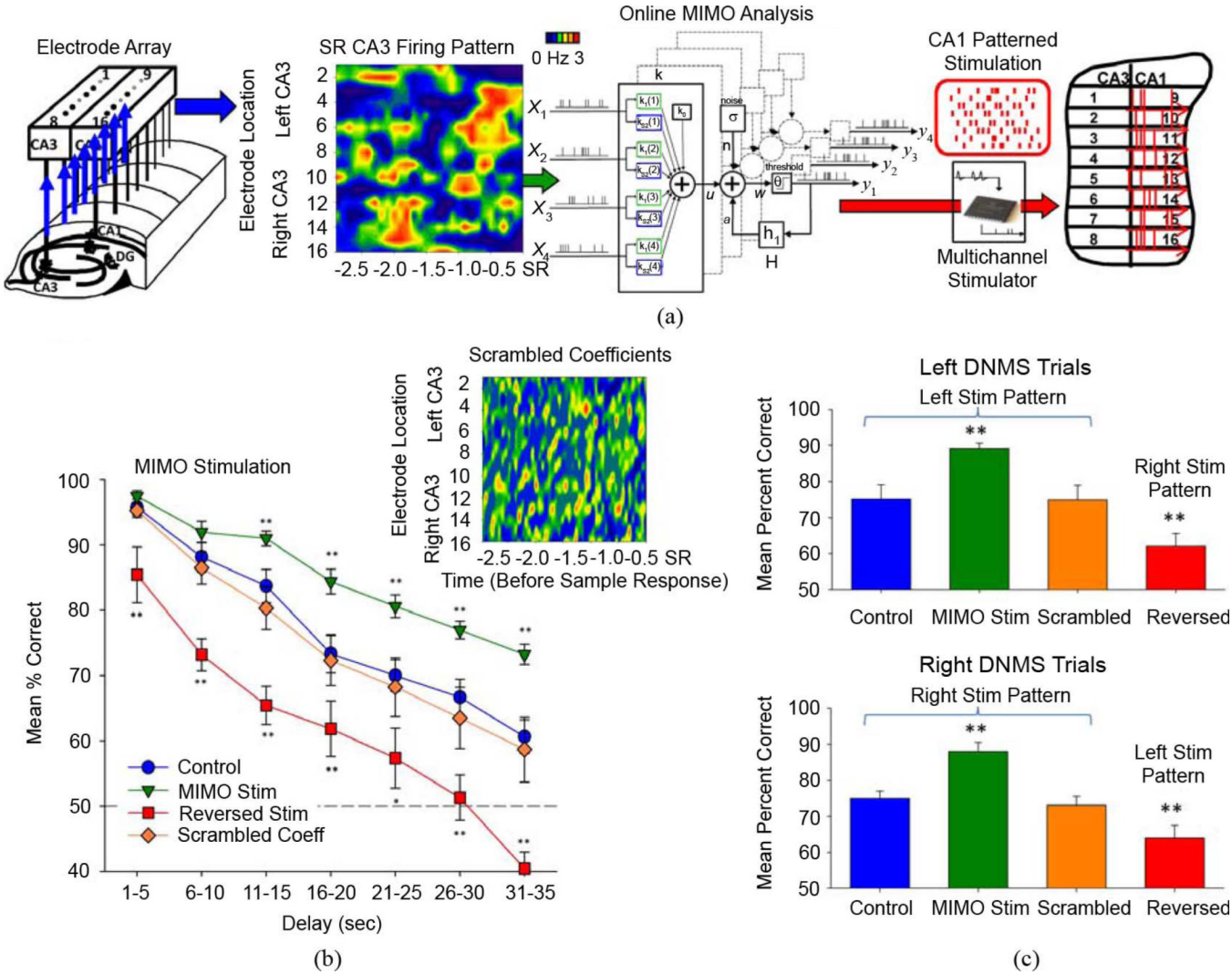

Fig. 3.

MIMO stimulation on DNMS trials. (a) Prediction of strong SR encoding in CA1 via MIMO model used to derive spatio-temporal patterns of electrical stimulation delivered to CA1 electrode sites (right). Stimulation consisted of biphasic electrical pulses (0.5–2.0 V, 10–50 μV, 0.5 s duration, minimum interpulse interval=50 ms), delivered on trials with delay durations of 15–50 s. (b) DNMS delay curves for animals (n = 9) tested under normal (no stimulation) conditions, and when 35% of trials received CA1 stimulation commencing 3.0 s prior to the SR. Stimulation sessions consisted of (a) CA1 patterns derived from the MIMO model (green), (b) reversal of patterns to deliver Right trial stimulation on Left trials, and vice versa (red), or (c) the same stimulation "power," but with randomization of MIMO coefficients to disrupt CA1 spatiotemporal firing patterns. Mean (±S.E.M.) DNMS performance is shown averaged over five sessions (i.e., 500 trials) per condition. Asterisks (*$p < 0.01$, **$p < 0.001$) indicate significant difference in DNMS performance compared to Control (No Stim.) trials. Inset: Weighted CA1 firing plot derived from strong-code DNMS trials when the MIMO coefficients were "scrambled" by randomizing the spatiotemporal sequence of coefficients (by neuron and time), but not the actual CA1 firing. (c) Same data as in B sorted according to Left versus Right DNMS trials. Bars indicate mean (±S.E.M.) DNMS performance averaged over all delays, dark shading=Left DNMS trials, light

shading=Right DNMS trails. Asterisks (**$p < 0.001$) indicate significant difference in DNMS performance compared to Control (No Stim.) trials.

NIH-PA Author Manuscript
NIH-PA Author Manuscript
NIH-PA Author Manuscript

NIH-PA Author Manuscript
NIH-PA Author Manuscript
NIH-PA Author Manuscript

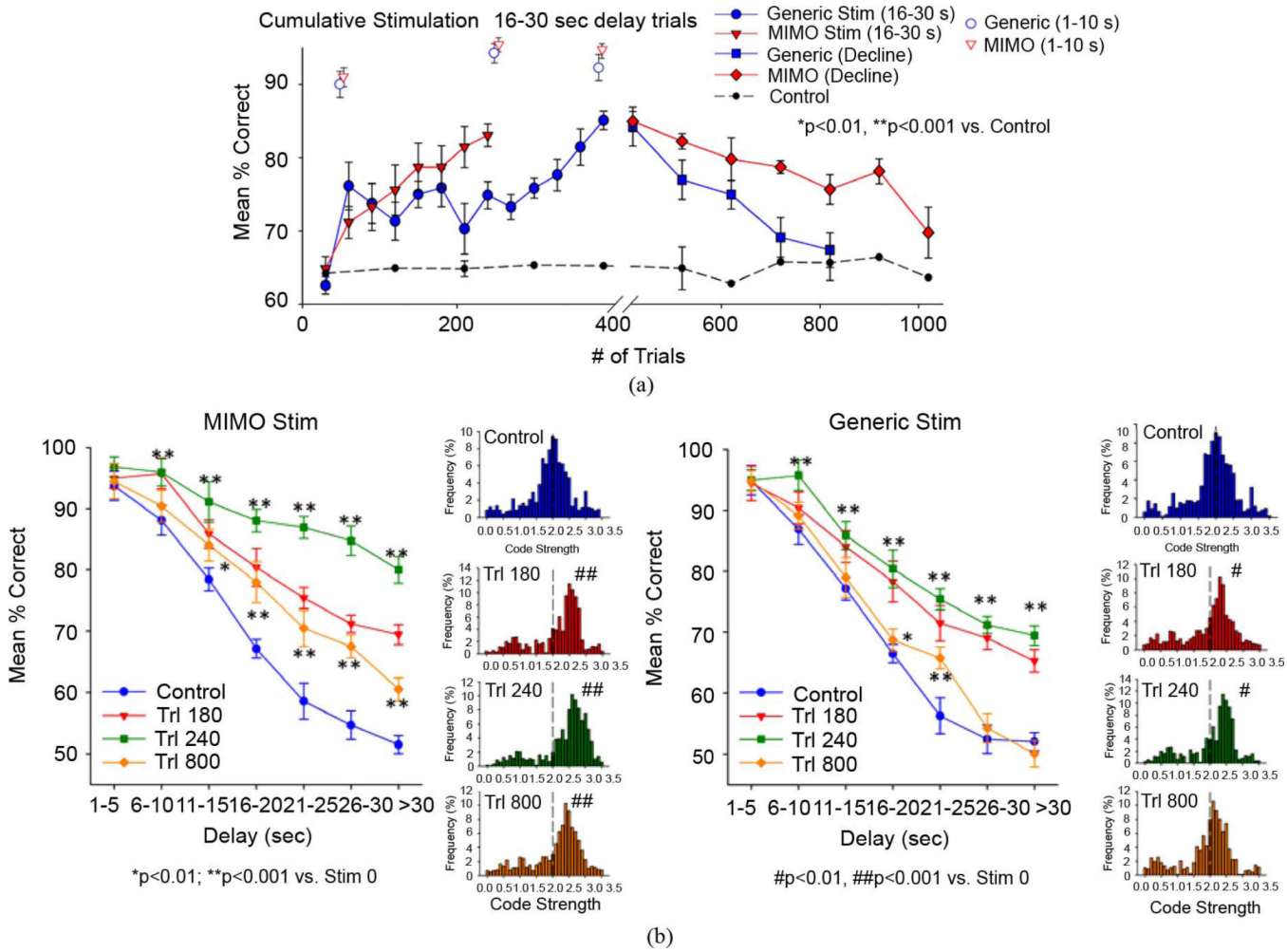

Fig. 4.

Cumulative effects of MIMO generated *strong* SR code CA1 stimulation. (a) Cumulative increase (left) in overall performance on nonstimulated trials (mean%correct ± SEM) in animals ($n = 8$) receiving 25–30 stimulation trials (Stim Trials) per session over successive sessions. Individualized MIMO stimulation patterns produced a more rapid increase in performance after 240 trials than Generic stimulation patterns that took an additional 160 trials (400 trials total) to produce equivalent performance levels (shown at breakpoint in axis). The right half of the plot (after the break point) shows the decay (Decline) of facilitated performance over an additional 600 trials with the same delays when stimulation was no longer delivered on any trials during the sessions. Dashed line=performance of equivalently trained animals ($n = 20$) that never received stimulation. (b) DNMS delay curves for phases of cumulative facilitation and decline in performance following 180 trials (Trl 180) and 240 trials (Trl 240) of MIMO (left) and Generic (right) stimulation and after cessation of stimulation for an additional 400 trials (Trl 800), corresponding to the periods shown in A. Distribution of SR code strengths for all trials within the same sessions are shown in the graphs to the right of the corresponding delay curves. Code Strength computed from overall ensemble firing rate multiplied by the MIMO coefficients for each trial (see Section II). Dashed vertical line indicates median code strength of 2.0 obtained prior to cumulative stimulation procedure. Asterisks (*$p < 0.01$, **$p < 0.001$) indicate significant

increase over control (no stimulation, Trl 0); hash marks (# $p < 0.01$, ##$p < 0.001$) indicate significant difference in code distribution from control (Trl 0).

NIH-PA Author Manuscript
NIH-PA Author Manuscript
NIH-PA Author Manuscript

NIH-PA Author Manuscript

NIH-PA Author Manuscript

NIH-PA Author Manuscript

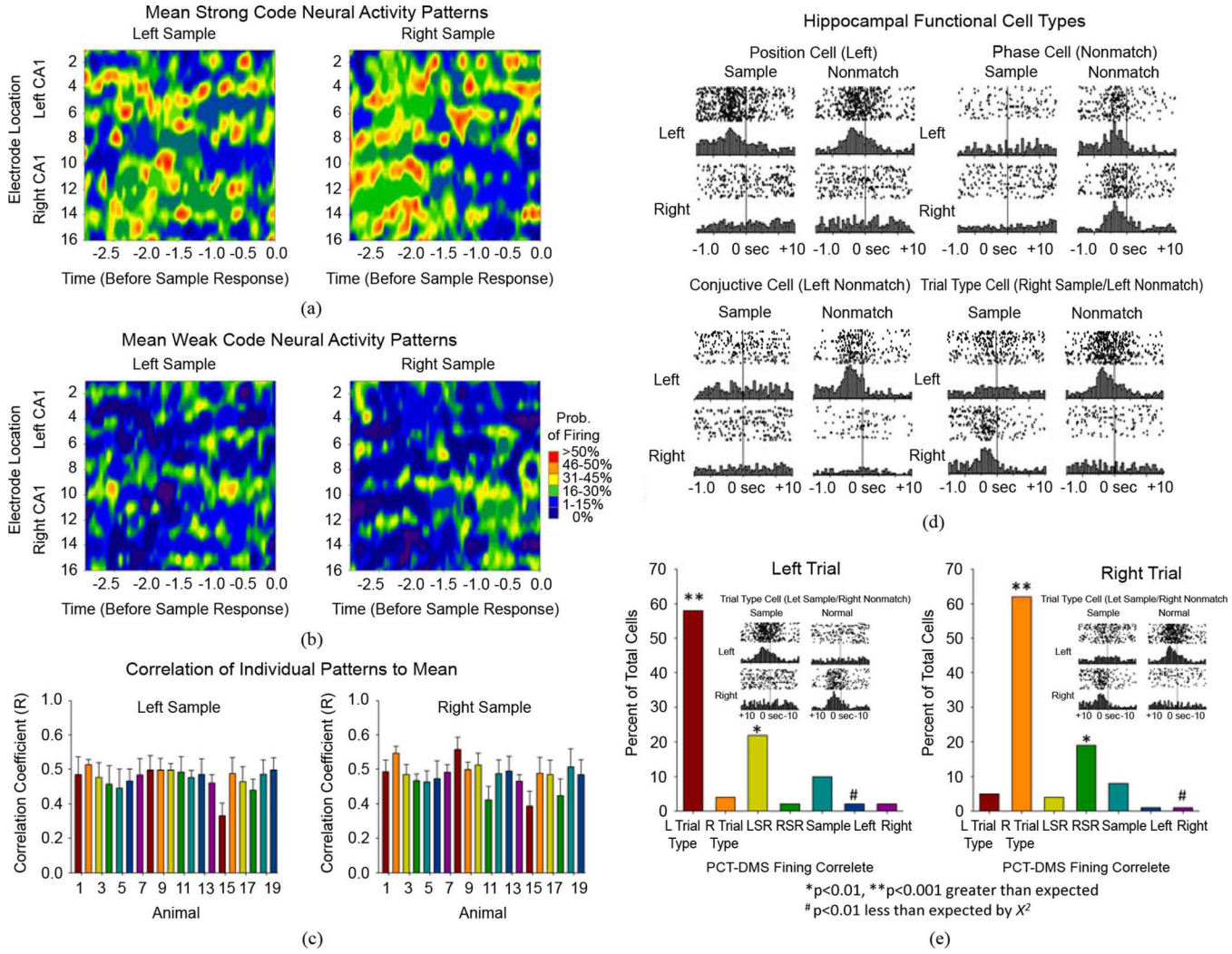

Fig. 5.

Neural contributions to MIMO model. (a) Mean firing rate contour maps of hippocampal ensemble activity averaged across 20 animals from neurons recorded at each respective CA1 electrode location in arrays in both hemispheres. Mean of MIMO derived *strong* SR codes calculated 3.0 s prior to SR occurrence (−3.0 to 0.0 s, X- axis) for left and right lever positions appropriate to the two types of DNMS trial. (b) Mean firing rate contour maps averaged across the same 20 animals as in A for MIMO derived *weak* SR codes. High density of firing in *strong* SR codes. (A) contrasts sharply with lack of firing density in *weak* SR codes. (B) averaged across the same animals and DNMS sessions. (c) Cross-correlation of each of the 20, single animal, *Strong* SR Code patterns with the mean pattern in A averaged over the remaining 19 animals. Distribution of high correlations ($R > 0.38$, $p < 0.001$) reveals consistent pattern of SR firing across animals, leading to identification of "Generic" MIMO *strong* SR codes for Left and Right lever trials. (d) Examples of FCTs recorded in hippocampal ensembles, shown as single trial raster displays (dots = neural spikes, row of dots = one DNMS trial,) and perievent histograms for ±1.5 s relative to SR and NR responses designated as 0.0 s. *Position* cells fire only to behavioral responses on one lever position (Left Position cell shown) in either phase of DNMS task. *Phase* cells fire only during Sample or Nonmatch phase, irrespective of position of lever response (Nonmatch phase cell shown). *Conjunctive* cells fire only to a particular combinations of position and

NIH-PA Author Manuscript

NIH-PA Author Manuscript

NIH-PA Author Manuscript

phase (i.e., Left Nonmatch cell shown). *Trial-type* cells combine conjunctive cell attributes and fire in both Sample and Nonmatch phases of task but only on a single type of trial and do not fire on the opposite type of trial (Right Sample/ Left Nonmatch *Trial-type* cell shown). (e) Contribution of FCTs to mean *strong* SR code in A. Individual ensembles exhibiting *strong* SR code patterns for 20 animals were analyzed, and neurons with a significant tendency to fire in this pattern (i.e., significant variance contributions: > 50% coefficient weighting) were classified as to FCT and ranked in terms of percentage of total cells contributing to the *strong* SR code pattern. Graphs indicate frequency distribution of different FCTs contributing to Left and Right *strong* SR codes in A. Asterisks (*$p < 0.01$, **$p < 0.001$) indicate significantly higher than chance contribution of a given FCT ($x^2_{(18)}>42.6$, $p < 0.001$); hash marks (#$p < 0.01$) indicate significantly lower contribution than expected by chance ($x^2_{(18)}=35.8$, $p < 0.01$).